A UAV-UGV Cooperative System: Patrolling and Energy Management for Urban Monitoring

Omar Sami Oubbati, *Member, IEEE*, Jamal Alotaibi, Fares Alromithy, Mohammed Atiquzzaman, *Senior Member, IEEE*, and Mohammad Rashed Altimania

***Abstract*—Urban monitoring in 6th Generation (6G) networks is vital for ensuring smart city security and efficiency. Traditional methods rely on either standalone Unmanned Aerial Vehicles (UAVs) or Unmanned Ground Vehicles (UGVs), often suffering from limited coverage, intermittent connectivity, and inefficient energy management. Recent works have explored UAV-UGV collaboration to enhance surveillance and communication; however, they lack dynamic communication optimization and energy-efficient coordination. To address these gaps, we propose a novel cooperative framework integrating UAVs equipped with Reconfigurable Intelligent Surfaces (RIS) and UGVs for real-time monitoring. Unlike prior approaches, our system optimizes UAV flight paths and recharging schedules using Deep Reinforcement Learning (DRL) while refining UGV patrol routes with a Genetic Algorithm (GA), ensuring adaptive and continuous surveillance. Additionally, we employ Differential Evolution (DE) for RIS configuration, enhancing data transmission and mitigating urban signal degradation. UAVs further support UGVs by wirelessly recharging them via energy beamforming, reducing dependency on fixed charging stations. By leveraging AI-driven coordination, RIS-assisted communication, and real-time energy optimization, our framework ensures seamless data transmission, reduces latency, and maximizes energy efficiency. Simulation results demonstrate that our approach significantly improves communication reliability, monitoring coverage, and energy consumption compared to existing methods, making it a promising solution for next-generation urban monitoring.**

***Index Terms*—Reconfigurable Intelligent Surfaces (RISs); 6G; Urban Monitoring; UAV; UGV; Energy Efficiency.**

I. Introduction

In the era of 6th Generation (6G) networks, advanced urban monitoring systems are increasingly critical due to the growing complexity and density of smart cities [1]. Real-time detection and response to Unusual Events (UVs) rely heavily on wireless communications to enable seamless data transmission between monitoring devices and central control systems, which is essential for public safety and efficient management [2]. However, dense urban infrastructures often disrupt wireless communications by causing signal blockages [3]. To overcome these challenges, integrating Unmanned Ground Vehicles (UGVs) and Unmanned Aerial Vehicles (UAVs), equipped with Optical and Infrared Cameras and powered by AI-based data processing, offers an effective solution. UGVs patrol autonomously, detecting and reporting UVs to a central controller via UAV-based relays. UAVs, equipped with Reconfigurable Intelligent Surface (RIS) technology, optimize signal propagation, ensuring reliable communication between UGVs and the central controller. Additionally, UAVs monitor areas inaccessible to UGVs, such as elevated roads and narrow streets, enhancing real-time urban monitoring where traditional systems fail.

Urban environments, with their dense infrastructures and obstacles, present significant challenges for maintaining reliable communication and monitoring in 6G networks [4]. Traditional methods, such as static ground-based sensor networks and conventional wireless systems, often fail in these environments due to limited flexibility and signal degradation caused by tall buildings and other urban obstructions [5], [6]. These challenges are particularly pronounced in high-density or disaster-prone areas where timely transmission of critical information is essential. Although 6G networks offer improved connectivity and real-time data processing, managing energy consumption and ensuring adaptability in dynamic urban environments remain significant challenges [7]. UAVs, in particular, rely on limited battery resources, leading to communication interruptions during extended missions [8], while UGVs have to optimize their patrol routes to cover high-risk areas without depleting energy reserves [9]. Prior research, such as Cao *et al.* [10], has explored dynamic UAV path planning to adjust trajectories based on energy availability, while multi-agent coordination algorithms [11] and hybrid machine learning methods [12] have been developed to optimize energy consumption in UAV-UGV operations. However, these strategies often struggle in unpredictable urban environments, where obstacles and rapidly changing conditions can disrupt even the most well-planned missions. Effectively managing both energy consumption and communication reliability in such settings is essential to fully realize the potential of 6G networks for urban monitoring.

To address the challenges of energy management, adaptability, and real-time UV detection in urban monitoring systems, as depicted in Fig. 1, we propose a novel framework deploying UAVs, exemplified by the EHang 184 for its high energy capacity. Initially designed for human transport, these UAVs are repurposed here for real-time urban monitoring, enabling wireless recharging of UGVs and efficient communication. UGVs patrol and detect UVs

O.S. Oubbati is with LIGM, University Gustave Eiffel, Marne-la-Vallée, France. E-mail: omar-sami.oubbati@univ-eiffel.fr

J. Alotaibi is with the department of computer engineering, College of Computer, Qassim University, Buraydah, Saudi Arabia. Email: j.alotabi@qu.edu.sa

F. Alromithy and M. R. Altimania are with the electrical engineering department, University of Tabuk, Tabuk, Saudi Arabia. Emails: {falromithy,moh-doshan}@ut.edu.sa

M. Atiquzzaman is with the University of Oklahoma, Norman, OK USA. E-mail: atiq@ou.edu

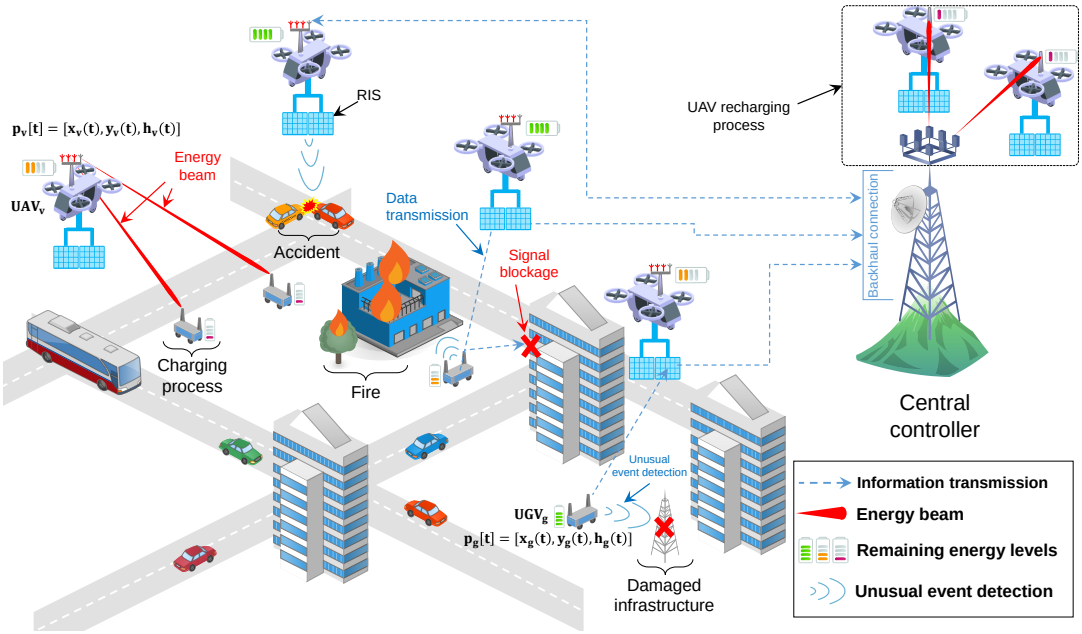

Fig. 1: Our framework's motivating scenario.

using optical and infrared cameras, capturing visual and thermal data for analysis. When UGV batteries fall below a critical threshold, they request recharging, prompting UAVs to wirelessly recharge them, ensuring continuous UGV operation. UAVs return to the central controller for recharging when their own batteries deplete, with recharging schedules managed to ensure uninterrupted monitoring. UAVs also monitor areas inaccessible to UGVs, such as elevated roads and narrow alleys, ensuring comprehensive coverage. UAV-mounted RISs dynamically adjust flight paths to maintain communication with UGVs, even in obstructed environments where obstacles may obstruct direct lines of sight. This framework ensures both UAVs and UGVs adapt to environmental changes, maintaining efficient operations and reliable UV detection throughout missions. While numerous studies explore UAV-UGV collaboration for urban monitoring, few—if any—holistically integrate intelligent communication, adaptive energy management, and AI-driven optimization in a unified framework. This work presents the following key contributions:

- This work introduces a novel UAV-UGV cooperative framework that integrates RIS-assisted UAVs to enhance urban communication reliability. Unlike traditional models, our approach reduces signal degradation in dense environments by leveraging intelligent RIS beamforming, ensuring seamless data transmission.
- A wireless UAV-based recharging system is proposed, replacing conventional fixed charging stations with dynamic energy beamforming. UAVs continuously recharge UGVs in real time, optimizing energy allocation and ensuring uninterrupted operations in mission-critical environments.
- AI-driven path optimization and energy management strategies are employed to enhance the efficiency of UAVs and UGVs. A Deep Reinforcement Learning (DRL) model based on Proximal Policy Optimization (PPO) optimizes UAV trajectory planning, while a Genetic Algorithm (GA) is used for adaptive UGV path planning, ensuring maximal energy efficiency and extended mission endurance.
- To further enhance communication efficiency in urban settings, we incorporate Differential Evolution (DE) for RIS phase shift optimization. This technique enables UAVs to dynamically adjust RIS configurations, improving signal propagation and mitigating interference, particularly in challenging, obstacle-dense environments.

The remainder of this paper is organized as follows: Section II provides an in-depth review of related works in urban monitoring. Section III outlines the core elements of the proposed framework. Section IV presents the problem formulation and optimization techniques applied to enhance system performance. Section VI discusses the results of our simulations. Finally, Section VII concludes the paper.

II. Related Work

The integration of UAV-mounted RISs and UGVs for urban monitoring and communication has gained significant attention with the advent of 6G networks [13]. Research has primarily focused on challenges such as energy management, communication reliability in dense urban environments, and optimizing cooperative frameworks between UAVs and UGVs. This section reviews key contributions in three main areas: (i) energy-efficient UAV-UGV systems, (ii) RISs in UAV-assisted networks, and (iii) optimization techniques for UAV-UGV cooperation, highlighting major advancements and ongoing challenges in each domain. At the end of this analysis, we synthesize the limitations of these contributions, clarifying how our work addresses these gaps effectively.

A. Energy-Efficient UAV-UGV Systems

Energy management in UAV-UGV systems is crucial for ensuring efficient collaboration and prolonged mission endurance. For instance, Li *et al.* [14] developed a dynamic scheduling and path-planning algorithm to reduce energy consumption in UAV-UGV collaborative missions, ensuring seamless coordination between vehicles. In [15], a UAV-assisted path-planning system is proposed that uses Disciplined Convex-Concave Programming (DCCP) to create energy-efficient routes for UGVs, particularly in complex environments. The authors of [16] introduced a system combining UAV and UGV data to create energy-efficient traversability maps, using aerial images and ground sensor data to minimize energy consumption.

B. RISs in UAV-Assisted Networks

RISs have emerged as a promising technology to enhance communication efficiency in UAV-assisted networks. Several studies have explored different aspects of RIS integration into UAV systems, focusing on energy efficiency, trajectory optimization, and resource management. In [17], the authors proposed an energy harvesting scheme using a DRL algorithm to optimize resource allocation in UAV-RIS networks, improving both energy harvesting and communication quality. The authors of [18] introduced a joint optimization framework for resource allocation and UAV trajectory in RIS-assisted mobile edge computing systems, significantly enhancing energy efficiency. Finally, Wang *et al.* [19] explored the use of a target-mounted RIS for joint location and orientation estimation, optimizing phase shifts and UAV positions to improve data collection accuracy.

C. Optimization Techniques for UAV-UGV Networks

Optimization techniques play a vital role in enhancing the performance of UAV-UGV networks, especially in dynamic and complex environments. Recent studies have focused on the development of optimization methods to manage path planning, resource allocation, and cooperation between UAVs and UGVs. For instance, Zhang *et al.* [20] proposed a cooperative approach where UAVs and UGVs work together in real-time for continuous data gathering while handling environmental challenges like obstacles and energy constraints. In [21], the authors explored informative trajectory planning, optimizing both UAV flight paths and UGV movements to maximize information collection . Finally, the authors of [22] presented a lightweight reinforcement learning (RL) solution aimed at real-time path planning for UAVs, offering a balance between computational efficiency and path optimization.

D. UAV-Assisted Networking and Distributed Learning in 6G

The integration of UAV-assisted networking and distributed learning is advancing in 6G, improving communication efficiency and decision-making. UAVs are essential for traffic offloading in air-ground networks, alleviating congestion and enhancing network performance. Fan *et al.* [23] proposed a scheme that optimizes load balancing and UAV rewards using a two-layer network graph model and a deep neural network-based genetic algorithm to improve decision-making. Lam *et al.* [24] developed a multimedia content delivery framework in UAV-assisted IoT networks, incorporating caching, power allocation, and 3D trajectory optimization to reduce latency and improve service quality. Distributed foundation models are also gaining attention for multi-modal learning in 6G [25]. Li *et al.* [26] introduced a deep learning framework for cross-modal object detection in UAV networks, improving detection and recognition across different sensing modalities.

Despite progress in energy management, RIS integration, UAV-UGV optimization, and UAV-assisted networking, challenges remain. Real-time adaptive energy optimization is vital in dynamic urban environments, and UAVs require better scheduling to minimize downtime. While RIS-equipped UAVs improve communication, scalability issues persist in complex terrains. UAVs' coverage of inaccessible areas and real-time detection also face challenges, especially in energy-efficient decision-making and cross-modal data integration. Although distributed learning and multi-modal AI offer new opportunities, their full potential in UAV-UGV systems is yet to be realized. In TABLE I, we compare our framework to previous systems, highlighting how our approach improves communication, energy distribution, and operational reliability through RIS-assisted UAVs, real-time recharging, AI-driven energy management, and adaptive RIS beamforming.

TABLE I: Our work vs. previous UAV-UGV systems

Feature	**Previous Work**	**Our Work**
UAV-UGV cooperation	Yes	Yes
UAV-based wireless UGV recharging	No	Yes (real-time energy beamforming)
RIS for UAV-assisted communication	No	Yes (RIS-enabled UAVs)
AI-driven UAV-UGV path optimization	Partial	Yes (DRL-based UAV trajectory, GA for UGV trajectory)
Energy management techniques	Basic	Yes (adaptive energy allocation)
RIS phase shift optimization	No	Yes (DE for dynamic beamforming)

Our proposed system addresses these gaps by leveraging a combined approach based on DRL and GA to optimize energy management, communication reliability, and UV detection. Both UAVs and UGVs are equipped with optical and infrared cameras for comprehensive monitoring, while UAVs are further optimized for recharging and monitoring coverage of inaccessible areas. The integration of RIS technology enhances communication reliability and scalability for large-scale deployments, ensuring effective relaying of detected UVs. A detailed comparison of our system with some discussed solutions in the subsections of Section II is highlighted in Table II, which shows its advantages in energy efficiency, communication reliability, and adaptability.

TABLE II: Comparative analysis of contributions.

		EE	CR	AD	Objective	Advantage	Drawback
Energy-Efficient Systems	Ref. [14]	√	×	Low	Reducing energy consumption in UAV-UGV collaborative missions.	Efficient energy management with path optimization.	Limited adaptability in dynamic environments.
	Ref. [15]	√	×	Moderate	Optimizing energy-efficient UGV routes in complex terrain.	Effective energy reduction in challenging environments.	Suboptimal communication reliability.
RIS-Assisted Networks	Ref. [17]	√	√	Moderate	Enhancing energy harvesting and improving communication quality in UAV-RIS systems.	Optimized resource allocation and energy efficiency.	Limited adaptability to changing environments.
	Ref. [18]	√	√	Moderate	Joint optimization of resource allocation and UAV trajectory.	Improves communication and energy management.	Complex to scale in larger networks.
Optimization Techniques	Ref. [20]	√	×	Moderate	Cooperative optimization for continuous data gathering in UAV-UGV networks.	Efficient real-time data collection.	Energy efficiency could be improved.
	Ref. [22]	×	√	High	Real-time path planning with lightweight RL.	Adaptable to dynamic environments with real-time adjustments.	Lower energy efficiency compared to other approaches.
UAV-Assisted and Distributed Learning	Ref. [23]	√	√	Moderate	UAV-enabled traffic offloading for network optimization.	Improves network congestion management and UAV task allocation.	Computational complexity in real-time environments.
	Ref. [26]	×	√	High	Cross-modal object detection in UAV networks.	Enhances object recognition through multi-modal learning.	High data processing overhead.
Our proposed solution		√	√	High	Optimizing UAV-UGV cooperation for monitoring, energy management, and communication reliability.	Enhanced energy efficiency, robust communication, and high adaptability to dynamic environments.	Increased complexity in system implementation.

EE: Energy Efficiency, **CR:** Communication Reliability, **AD:** Adaptability in dynamic environments.

III. System Model

As depicted in Fig. 1, we propose a UAV-UGV cooperative system integrated with RISs for enhanced urban monitoring and patrolling in smart cities. The system consists of three main components: (i) a fleet of autonomous UAVs equipped with RIS modules, denoted as $\mathcal{V} \triangleq \{v = 1, 2, \ldots, V\}$, (ii) a set of UGVs, denoted as $\mathcal{G} \triangleq \{g = 1, 2, \ldots, G\}$, and (iii) a central controller, which supervises and optimizes the system operations. The central controller plays a triple role: (i) optimizing UAV and UGV trajectories and communication, (ii) wirelessly supplying UAVs with energy via a base station located at the edge of the monitored square area of width $\mathbb{W}$, and (iii) evaluating each zone's risk priority for effective resource allocation. The later is conducted through the dynamic risk scoring method that continuously assesses each zone's priority using real-time UV detection data and historical Data. As risk levels change, UAVs and UGVs adjust their patrol focus to detect UVs (*e.g.,* accidents, damaged infrastructure, or vandalism) on high-risk zones through their embedded optical and infrared cameras. The detection of UVs is carried out using AI-based data processing algorithms, which are beyond the scope of this paper. Let $p_v[t] = [x_v(t), y_v(t), h_v(t)]$ represent the time-varying location of UAV v at time slot t, where $h_v(t)$ is its altitude. The position of UGV g at time t is denoted as $p_g[t] = [x_g(t), y_g(t), h_g(t)]$, where $h_g(t) = 0$ since UGVs operate on flat terrain. The distance between UAV v and UGV g at time t is calculated as:

$$d_v^g[t] = \sqrt{\|p_v[t] - p_g[t]\|^2}, \tag{1}$$

UAVs also serve as communication relays between UGVs and the central controller via their RIS modules, optimizing signal propagation in urban environments. Additionally, UAVs are equipped with wireless energy transmitters to recharge UGVs when their batteries drop below a threshold, ensuring uninterrupted operation. UAVs periodically return to the central controller's base station for recharging, with recharging schedules optimized by the central controller to maintain continuous monitoring. The movements of UAVs and UGVs, UAV recharging, and RIS configurations are fully controlled by the central controller, which runs optimization agents for all system components. The system operates over a finite interval $t \in [0, \varkappa]$, discretized into T time slots of duration $\Delta = \frac{\varkappa}{T}$. UAVs and UGVs execute an action within each time slot t, where $t \in \mathcal{T} \triangleq \{1, 2, \ldots, T\}$. During each time slot, the central controller evaluates system conditions and makes decisions on trajectory adjustments, risk prioritization, and energy management. The modular design of the ADVISE system ensures that each component—UAVs, UGVs, and the central controller—can be independently upgraded or maintained without affecting the overall operation. This architecture enables easy scaling, as additional UAVs or UGVs can be integrated without disruptions. Such modularity ensures long-term flexibility and efficient maintenance, while simplifying system upgrades and operational continuity. Furthermore, security is critical in UAV-UGV networks due to risks like data interception, cyber-attacks, and jamming. Lightweight encryption (e.g., ECC, AES) ensures secure communication, while authentication prevents unauthorized access. Physical-layer defenses include frequency hopping, beamforming, and interference mitigation. Though beyond this paper's scope, future work will explore AI-driven

intrusion detection and secure multi-agent communication for large-scale UAV-UGV systems. For clarity, Table III provides the definitions of the key notations used throughout this paper.

TABLE III: List of notations.

Notation	Description
$\mathcal{V}$, V, v	Set, Number, Index of UAVs
$\mathcal{G}$, G, g	Set, Number, Index of UGVs
$\mathcal{T}$, T, t	Set, Number, Index of time-slots
$d_i^j[t]$	Distance between devices i and $j \in \mathcal{V} \cup \mathcal{G}$
$p_v[t]$	Position of UAV v, where $v \in \mathcal{V}$
$p_g[t]$	Position of UGV g, where $g \in \mathcal{G}$
$E_i[t]$	Residual energy of device $i \in \mathcal{V} \cup \mathcal{G}$
$\chi_i^j[t]$	Time-varying channel gain between devices i and $j \in \mathcal{V} \cup \mathcal{G}$
$P_i[t]$	Transmission power of device $i \in \mathcal{V} \cup \mathcal{G}$
$\psi_i[t]$	Risk score of zone i
$R_g[t]$	Data rate of UGV $g \in \mathcal{G}$
$z_i^{g,v}[t]$	Occupancy status of zone i by UAV v or UGV g
$r_v[t]$	Reward obtained by UAV $v \in \mathcal{V}$
$o_v[t]$	Environment observation of UAV $v \in \mathcal{V}$
$a_v[t]$	Action taken by UAV $v \in \mathcal{V}$
$A_v[t]$	Advantage function of agent $v \in \mathcal{V}$
σ_v	Actor parameter of agent $v \in \mathcal{V}$
ω_v	Critic parameter of agent $v \in \mathcal{V}$

A. Transmission Model

Each component in the UAV-UGV cooperative system is equipped with specialized antennas for energy transmission, UV detection, and communication. UAVs are equipped with: (i) an $M \times N$ Uniform Planar Array (UPA) antenna for energy beamforming to recharge UGVs, (ii) a RIS with a $K \times L$ UPA of passive reflecting elements for enhancing signal propagation by adjusting the phase-shift matrix $\mathbf{\Theta}$, and (iii) a directional antenna for UV data transmission and receiving energy during recharging. UGVs utilize two antennas on orthogonal frequency bands, one for transmitting UV data and charging requests, and the other for receiving energy, ensuring minimal interference between communication and energy transfer. Data transmission from UGVs to the central controller, either through UAV-RISs or directly, employs Non-Orthogonal Multiple Access (NOMA) [27], with Successive Interference Cancellation (SIC) at the central controller to mitigate interference and ensure reliable communication.

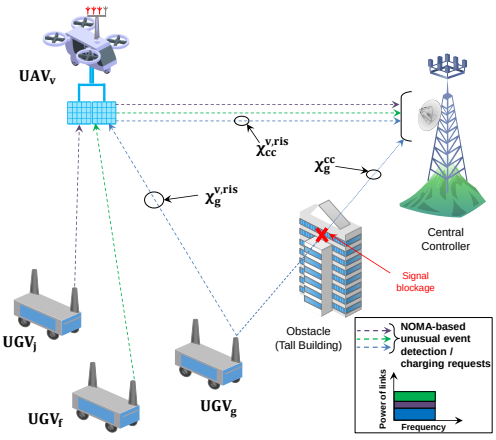

Fig. 2: UV and charging request transmission.

1) Transmission of detected UVs and charging requests: Efficient transmission of UVs and charging requests is crucial for continuous operations. NOMA enables UGVs to share the same frequency band, with weaker channels prioritized for decoding, and SIC at the central controller [28] cancels interference from stronger channels. After decoding weaker signals, stronger ones are decoded as their interference is eliminated. As shown in Fig. 2, transmissions occur directly or via UAV-mounted RISs, where each RIS element applies a phase shift, $\mathbf{\Theta} = \text{diag}(e^{j\theta_1}, e^{j\theta_2}, \ldots, e^{j\theta_{KL}})$, with θ_i being the phase shift of the i-th RIS element. The time-varying channel gain $\chi_g^{cc}[t]$ between UGV g and the central controller is modeled as in [29], [30].

$$\chi_g^{cc}[t] = \sqrt{\zeta_0 d_g^{cc}[t]^{-\alpha}} \left(\sqrt{\frac{\hat{K}}{1+\hat{K}}} \chi_g^{cc,\text{LoS}}[t] + \sqrt{\frac{1}{1+\hat{K}}} \chi_g^{cc,\text{NLoS}}[t] \right), \tag{2}$$

where ζ_0, $\alpha \geq 2$, and $\hat{K}$ represent the reference gain at distance d_0 =1m, path loss exponent, and Rician factor, respectively. The terms $\chi_g^{cc,\text{LoS}}[t]$ and $\chi_g^{cc,\text{NLoS}}[t]$ correspond to the deterministic LoS and scattered NLoS components, respectively. As in [31], the direct channel data rate for UGV g is given by:

$$R_g^{cc}[t] = B \log_2 \left(1 + \frac{P_g[t] \cdot |\chi_g^{cc}[t]|^2}{\sum_{i=1}^{g-1} P_i[t] \cdot |\chi_i^{cc}[t]|^2 + N_0} \right), \tag{3}$$

Where B is the available bandwidth, $P_g[t]$ is the transmit power of UGV g at time t, N_0 is the noise power, and the sum $\sum_{i=1}^{g-1} P_i[t] \cdot |\chi_i^{cc}[t]|^2$ represents interference from other UGVs in the NOMA decoding process. For RIS-assisted transmissions, the channel gain $\chi_g^{v,\text{RIS}}[t]$ between UGV g and UAV v is modeled similarly to the direct channel $\chi_g^{cc}[t]$, while the channel gain $\chi_{cc}^{v,\text{RIS}}[t]$ between the central controller and UAV v includes only the LoS component. The data rate is expressed as in [32].

$$R_g^{v,\text{RIS}}[t] = B \log_2 \left(1 + \frac{P_g[t] \cdot |\chi_g^{v,\text{RIS}}[t] + \mathbf{\Theta} \chi_{cc}^{v,\text{RIS}}[t]|^2}{\sum_{i=1}^{g-1} P_i[t] \cdot |\chi_i^{v,\text{RIS}}[t] + \mathbf{\Theta} \chi_{cc}^{v,\text{RIS}}[t]|^2 + N_0} \right), \tag{4}$$

where $\sum_{i=1}^{g-1} P_i[t] \cdot |\chi_i^{v,\text{RIS}}[t] + \mathbf{\Theta} \chi_{cc}^{v,\text{RIS}}[t]|^2$ represents the cumulative interference from other UGVs with stronger channels (ranked higher in NOMA decoding). The total data rate for UGV g at time t is the sum of the RIS-assisted and direct rates:

$$R_g[t] = \sum_{v=1}^{V} \aleph_g^v[t] R_g^{v,\text{RIS}}[t] + R_g^{cc}[t], \tag{5}$$

where $\aleph_g^v[t] \in \{0, 1\}$ is a binary variable that indicates the coverage status of UGV g by UAV v. $\aleph_g^v[t]$ is set to 1 if $R_g^{v,\text{RIS}}[t] \geq \tau$, where τ is the minimum required threshold to meet the Quality of Service (QoS). Otherwise, $\aleph_g^v[t]$ is set to 0. To further maximize $R_g[t]$, the system should maximize the sum of data rates for all UGVs. The optimization problem is defined as:

$$\max_{\{\mathbf{\Theta}\}} \sum_{g=1}^{G} R_g[t] \tag{6}$$

s.t.

$$\textbf{C1:} \quad \theta_i \in [0, 2\pi], \quad \forall i \in \{1, 2, \ldots, KL\}.$$

Constraint **C1** ensures that RIS phase shifts stay within the valid range of $[0, 2\pi]$, which is essential for proper signal reflection and optimal data transmission performance. Practical factors like energy constraints, communication reliability, and system scalability are implicitly addressed in the optimization via the data rate maximization objective. While not explicitly formulated, these constraints are managed by the optimization framework through overall performance maximization. The Differential Evolution (DE) algorithm [33] shown in Algorithm 1 is used to optimize the phase-shift matrix $\boldsymbol{\Theta}$ in real-time, maximizing the data rate. A population of candidate RIS configurations is initialized, and for each generation, new candidates are generated via mutation and crossover. Trial solutions are evaluated based on the data rate $R_g[t]$, and the best configurations are selected for the next generation. This process continues until the optimal RIS configuration $\boldsymbol{\Theta}^*$ is found, which maximizes the data rate. The optimization is repeated at each time slot t to adapt to changing channel conditions.

Algorithm 1: DE-based Optimization for RIS Phase-Shift Configuration

Input: Initial population $\{\boldsymbol{\Theta}^{(1)}, \ldots, \boldsymbol{\Theta}^{(S)}\}$
Initialize: Population size S, mutation factor F, crossover rate CR, max generations $X_{\max}$
for each generation $x = 1$ to $X_{\max}$ **do**
  for each candidate $\boldsymbol{\Theta}^{(i)}$ **do**
    Mutation: Generate mutant vector $\mathbf{V}^{(i)} = \boldsymbol{\Theta}^{(r1)} + F(\boldsymbol{\Theta}^{(r2)} - \boldsymbol{\Theta}^{(r3)})$
    Crossover:
    for each dimension j of $\boldsymbol{\Theta}^{(i)}$ **do**
      Generate a random number $r \in [0, 1]$
      if $r \leq CR$ **then**
        Set $\mathbf{U}_j^{(i)} = \mathbf{V}_j^{(i)}$
      else
        Set $\mathbf{U}_j^{(i)} = \boldsymbol{\Theta}_j^{(i)}$
      end if
    end for
    Selection: Evaluate data rate $R_g[t]$ for $\mathbf{U}^{(i)}$ and $\boldsymbol{\Theta}^{(i)}$
    Select $\boldsymbol{\Theta}^{(i+1)} = \mathbf{U}^{(i)}$ if $R_g[t](\mathbf{U}^{(i)}) > R_g[t](\boldsymbol{\Theta}^{(i)})$, otherwise retain $\boldsymbol{\Theta}^{(i)}$
  end for
end for
Output: Optimal RIS configuration $\boldsymbol{\Theta}^*$

2) UGV Energy Harvesting: As shown in Fig. 3, UGVs are equipped with energy harvesting units to receive energy wirelessly from UAVs. Each UGV g has a dedicated antenna for energy reception, allowing recharging during patrols without returning to a fixed station. When a UGV's battery falls below a threshold, it sends a charging request to UAVs within range, prompting the deployment of targeted charging beams. UAVs, equipped with an $M \times N$ UPA antenna, generate multiple energy beams to recharge UGVs. UGVs convert received Radio Frequency (RF) energy into usable power via onboard RF-energy gathering devices, with beam angle fluctuations ignored to ensure stable transmission.

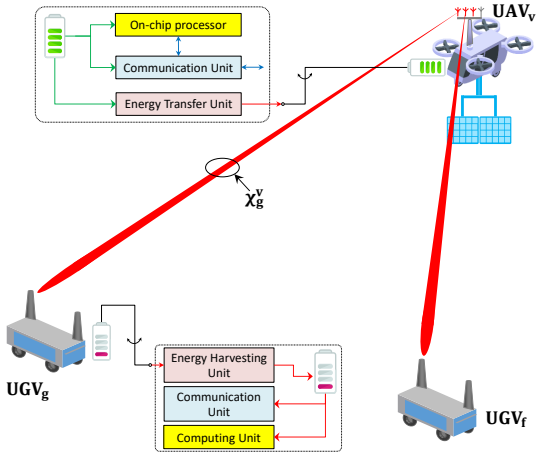

Fig. 3: Energy harvesting model.

The energy harvested by UGV g from UAV v depends on the channel gain $\chi_g^v[t]$, modeled using Rician fading as in [34], and is expressed as:

$$\chi_g^v[t] = \sqrt{\zeta_0 d_g^v[t]^{-\alpha}} \left(\sqrt{\frac{\hat{K}}{1+\hat{K}}} \chi_g^{v,\text{LoS}}[t] + \sqrt{\frac{1}{1+\hat{K}}} \chi_g^{v,\text{NLoS}}[t] \right). \tag{7}$$

The total energy harvested by UGV g from UAV v at time-slot t is given by:

$$E_g^v[t] = \xi \cdot P_v \cdot \Delta \cdot |r(\varphi, \Omega) BF|^2 \cdot |\chi_g^v[t]|^2, \tag{8}$$

where ξ is the energy conversion efficiency, P_v is the UAV's transmit power, BF is the beamforming vector, and $r(\varphi, \Omega)$ is the steering vector of the UPA antenna, with φ and Ω as azimuth and elevation angles. It is defined as $r(\varphi, \Omega) = \frac{1}{\sqrt{MN}}[1, e^{j\frac{2\pi}{\lambda} d(\sin(\Omega)\cos(\varphi))}, \ldots, e^{j\frac{2\pi}{\lambda} d((M-1)\sin(\Omega)\cos(\varphi)+(N-1)\sin(\Omega)\sin(\varphi))}]^T$, where $d(.)$ is the antenna element spacing, and λ is the wavelength. The energy harvesting model is linear to prevent circuit saturation. The beamforming vector controls the antenna elements to direct energy beams efficiently toward UGVs, ensuring stable transmission. The harvested energy is added to the UGV's energy level $E_g[t-1]$, and the total residual energy at time t is updated as:

$$E_g[t] = \begin{cases} E_g^{\max}, & \text{if } E_g[t-1] + \sum_{v=1}^{V} E_g^v[t-1] \geq E_g^{\max}, \\ E_g[t-1] + \sum_{v=1}^{V} E_g^v[t-1], & \text{Otherwise}, \end{cases} \tag{9}$$

During the charging process, UGVs and UAVs remain stationary until fully charged, ensuring stable energy transfer. Once recharged, UGVs and UAVs resume normal operations.

B. UAV Energy Consumption Model

UAV energy consumption covers four tasks: (i) hovering, (ii) movement, (iii) local video processing, and (iv) data

transmission upon UV detection. Hovering energy for UAV v, dependent on its weight (including RIS payload), is modeled as [35]:

$$E_v^{\text{hover}} = \frac{I_p \cdot W_v^{3/2}}{\sqrt{2 \cdot \varrho \cdot A_r}}, \tag{10}$$

where I_p is the induced power coefficient, W_v the UAV's total weight, ϱ the air density in kg/m^3, and A_r the rotor disk area in m^2. Movement energy, influenced by wind speed $V_{\text{wind}}(t)$, is given by [36]:

$$E_v^{\text{move}}[t] = \frac{1}{2} \cdot \varsigma_d \cdot \varrho \cdot A_f \cdot (V_v(t) + V_{\text{wind}}(t))^3, \tag{11}$$

where ς_d is the drag coefficient, A_f the frontal area, and $V_v(t)$ the UAV's velocity at time t. For local processing, energy depends on task size $S_v[t]$ and frequency f_v [37]:

$$E_v^{\text{comp}}[t] = \kappa_v \cdot F_v \cdot f_v^2 \cdot S_v[t], \tag{12}$$

where κ_v is the efficiency constant and F_v the CPU cycles per data bit. Thus, the residual energy of UAV v at $t+1$ is:

$$E_v[t+1] = E_v[t] - \left(\underbrace{\int_0^t E_v^{\text{hover}} + E_v^{\text{move}}[t]dt}_{\text{hovering and movement energy}} + \underbrace{\int_0^t \kappa_v F_v f_v^2 S_v[t]dt}_{\text{computation energy}} + \underbrace{\int_0^t \eta_v[t] P_v dt}_{\text{wireless power transfer energy}} + \underbrace{\int_0^t P_v \cdot T_v[t]dt}_{\text{communication energy}} \right), \tag{13}$$

where $T_v[t]$ is the data size transmitted and $\eta_v[t]$ indicates if UAV v is charging UGVs ($\eta_v[t] = 1$) or not ($\eta_v[t] = 0$).

C. UGV Energy Consumption Model

UGVs primarily consume energy in mobility, data processing, and communication, with negligible wind effects. Mobility energy based on rolling resistance [38] is:

$$E_g^{\text{move}}[t] = \frac{1}{2} \cdot \varpi_r \cdot M_g \cdot g \cdot V_g(t), \tag{14}$$

where ϖ_r is the rolling resistance, M_g the UGV mass, g the gravitational constant, and $V_g(t)$ the UGV's velocity at t. As with UAVs, computation energy depends on task size $S_g[t]$ and frequency f_g:

$$E_g^{\text{comp}}[t] = \kappa_g \cdot F_g \cdot f_g^2 \cdot S_g[t], \tag{15}$$

where κ_g is the energy efficiency constant and F_g is the number of CPU cycles required per bit of data. The residual energy of UGV g at $t+1$ is updated as:

$$E_g[t+1] = E_g[t] - \left(\underbrace{\int_0^t \frac{1}{2} \varpi_r M_g g V_g(t)dt}_{mobility\ energy} + \underbrace{\int_0^t \kappa_g F_g f_g^2 S_g[t]dt}_{computation\ energy} + \underbrace{\int_0^t P_g \cdot T_g[t]dt}_{communication\ energy} \right), \tag{16}$$

where $T_g[t]$ is the transmitted data size, capturing UGVs' total energy needs for optimized management.

D. Risk Priority Evaluation Algorithm

The monitored area is divided into Z zones, with each zone's risk priority dynamically evaluated in real-time to allocate UAV and UGV resources efficiently. Initially, the risk score for each zone i is based on historical data H_i (*e.g.,* past incidents) and updated during the mission using real-time camera data $C_i[t]$, capturing UVs such as crowds, accidents, or vandalism. The total risk score for zone i at time t, denoted by $\psi_i[t]$, is calculated as:

$$\psi_i[t] = C_i[t] + H_i, \tag{17}$$

Fig. 4 shows zones categorized by risk priority: (i) **High Risk (Red)** if $\psi_i[t] > 75\%$, (ii) **Medium Risk (Yellow)** if $50\% \leq \psi_i[t] \leq 75\%$, and (iii) **Low Risk (Green)** if $\psi_i[t] < 50\%$. Risk scores are continuously updated, with $C_i[t]$ increasing if a UV is detected or decreasing if no incidents occur, ensuring efficient UAV and UGV allocation to critical zones.

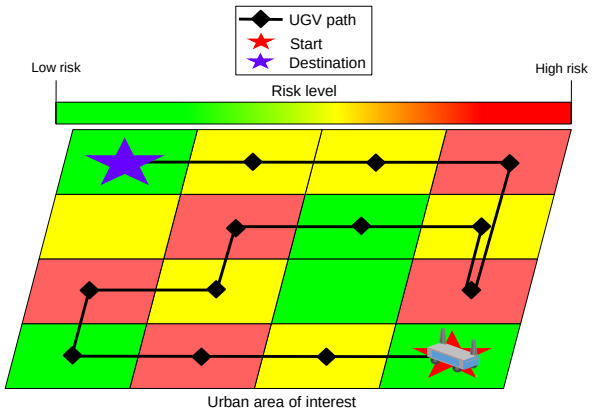

Fig. 4: Risk priorities and UGV path via Genetic Algorithm.

At each time-slot t, the risk score for each zone is dynamically updated based on new camera data from UAVs and UGVs. If a UV is detected in a low-risk zone, $C_i[t]$ increases, potentially raising the zone's risk category. Conversely, if no incidents occur over time, $C_i[t]$ may become negative, reducing the risk score. The risk score is recalculated at every time-slot to ensure UAV and UGV resources are allocated to the most critical zones in real-time. Algorithm 2 outlines the process.

To implement GA for UGV movement optimization in UAV networks, real-time data from UAVs and UGVs is essential for accurate path planning. As outlined in Algorithm 2, GA adapts to dynamic urban environments by continuously monitoring vehicle positions and environmental factors. Constraint **C2** ensures that no more than one UAV and one UGV visit the same zone simultaneously, enforced through real-time location tracking and path adjustments. Additionally, UAV-UGV communication protocols enable real-time data exchange, optimizing UGV routes while ensuring seamless coordination. Practical challenges such as communication delays, battery constraints, and dynamic

Algorithm 2: Risk Priority Evaluation Algorithm

Input: Set of zones Z, historical risk data H_i and current camera data $C_i[t]$ for each zone i at time t.
Initialize: Compute initial risk score $\psi_i[0] = C_i[0] + H_i$ for each zone i.
for each time-slot t **do**
  for each zone $i \in Z$ **do**
    Update $C_i[t]$ based on new UV detections.
    Recalculate the risk score: $\psi_i[t] = C_i[t] + H_i$.
    Classify zone i**:**
    if $\psi_i[t] > 75$ **then**
      Assign high-risk (Red) priority to zone i.
    else if $50 \leq \psi_i[t] \leq 75$ **then**
      Assign medium-risk (Yellow) priority to zone i.
    else
      Assign low-risk (Green) priority to zone i.
    end if
  end for
end for
Output: Updated risk scores $\psi_i[t]$ for each zone i.

obstacles are addressed through adaptive algorithms and hybrid optimization strategies, balancing local autonomy with centralized control for robust real-world deployment.

The central controller coordinates the UAV-UGV system by continuously processing real-time data from agents, including GPS-based positioning, energy levels, and environmental risks. UAVs and UGVs transmit this data via a reliable network, using UAV-mounted relays when needed. To minimize overhead, only critical information is prioritized. The controller dynamically adjusts UAV and UGV paths using optimization algorithms, ensuring real-time adaptability. Designed for resilience, the system mitigates communication delays through local optimizations, maintaining continuous operation in challenging environments.

IV. Problem Formulation and Optimization

In complex urban environments, coordinating UAVs and UGVs is essential for efficient monitoring, energy management, and task execution. The independent movement of UAVs and UGVs presents challenges in optimizing their paths to ensure timely UV detection and energy efficiency. This section formulates optimization problems for UAV and UGV movements to maximize coverage, minimize energy consumption, and improve communication. UGV movement optimization, using GA, focuses on covering high-priority zones and reducing energy consumption. UAV movement optimization, adapting to dynamic changes, is addressed using PPO, a reinforcement learning technique for real-time path learning. We chose PPO for UAV trajectory planning due to its ability to handle continuous action spaces and provide stable real-time updates in dynamic environments. Its strong exploration-exploitation balance makes it ideal for navigating complex urban settings. GA was selected for UGV route optimization due to its efficiency in combinatorial optimization, delivering near-optimal solutions for path planning with objectives like energy efficiency and coverage. Both algorithms are well-suited for multi-agent, dynamic scenarios, which is critical for UAV-UGV coordination in 6G networks.

The optimization problems presented form a cohesive UAV-UGV coordination strategy. Equation (6) optimizes RIS-equipped UAV phase shifts to improve communication reliability, directly affecting UGV data transmission. This complements Equation (18), which optimizes UGV movement for efficient coverage of high-risk zones while managing energy consumption. Equation (19) integrates UAV trajectory planning with recharging scheduling to ensure continuous operations. Together, these three formulations create an energy-aware, communication-optimized UAV-UGV framework for urban monitoring.

A. UGV Movement Optimization

UGVs aim to maximize coverage of high-risk zones while minimizing energy consumption. They adapt to real-time risk levels by prioritizing zones based on updated risk scores. The goal is to optimize the path between start and destination points using GA, minimizing time and energy spent patrolling high-risk zones. Once a UGV reaches its destination, the start and destination points are swapped, ensuring continuous patrols. GA-based dynamic path optimization allows UGVs to adapt to real-time risk levels, minimize travel distances, and meet energy constraints. Let $\mathcal{P}_G$ denote the UGV path, $\mathcal{Z}$ the set of all zones, and $\mathcal{G}$ the set of all UGVs. Define $z_i^{g,v}[t] \in \{0,1,2\}$ as the occupancy of zone i at time t, where $z_i^{g,v}[t] = 0$ means unvisited, $z_i^{g,v}[t] = 1$ means visited by one UGV or UAV, and $z_i^{g,v}[t] = 2$ means visited by both.

$$\max_{\{\mathcal{P}_G\}} \sum_{t=0}^{T} \sum_{i \in \mathcal{Z}} \sum_{(g,v) \in \mathcal{G} \times \mathcal{V}} z_i^{g,v}[t] \psi_i[t] + \left(\frac{\sum_{t=0}^{T} \sum_{g \in \mathcal{G}} E_g[t]}{G \cdot T} \right) \quad (18)$$

Subjected to:

$$\text{C1:} \quad z_i^{g,v}[t] \in \{0,1,2\}, \quad \forall i \in \mathcal{Z}, \forall t \in \mathcal{T}, \forall g \in \mathcal{G}, \forall v \in \mathcal{V},$$

$$\text{C2:} \quad \sum_{(g,v) \in \mathcal{G} \times \mathcal{V}} z_i^{g,v}[t] \leq 2, \quad \forall t \in \mathcal{T}, \forall i \in \mathcal{Z}$$

$$\text{C3:} \quad E_g[t] \geq E_g^{\min}, \quad \forall g \in \mathcal{G}, \forall t \in \mathcal{T},$$

$$\text{C4:} \quad \sum_{i \in \mathcal{Z}} z_i^{g,v}[t] \cdot \psi_i[t] \geq \psi_{\min}, \quad \forall g \in \mathcal{G}, \forall v \in \mathcal{V}, \forall t \in \mathcal{T}.$$

The objective of (18) is to maximize the total number of high-risk zones $z_i^{g,v}[t]\psi_i[t]$ visited by UAVs and UGVs, while considering each UGV's energy consumption. The variable $z_i^{g,v}[t]$ captures zone occupancy, where a zone can be occupied by at most one UGV and one UAV. **C1** enforces that $z_i^{g,v}[t]$ can be 0, 1, or 2, representing unoccupied, occupied by one vehicle, or both. **C2** ensures that no more than two devices (one UGV and one UAV) can visit the same zone. **C3** maintains the energy level $E_g[t]$ of each UGV g above a minimum threshold $E_g^{\min}$. **C4** prioritizes high-risk zones with $\psi_i[t] > \psi_{\min}$ in the UGV's patrol route. This problem is

effectively solved using GA [39] in ALgorithm 3, which is ideal for combinatorial optimization tasks like path planning.

Algorithm 3: Genetic Algorithm for UGV Movement Optimization

Input: Initial population of UGV paths $\mathcal{P}_G$, maximum generations $X_{\max}$
Initialize: Randomly generate a population of Y candidate paths $\{\mathcal{P}_G^1, \ldots, \mathcal{P}_G^Y\}$
for generation $x = 1$ to $X_{\max}$ **do**
  Evaluate the fitness of each path $\mathcal{P}_G^i$ using (18);
  Select the best-performing paths for reproduction
  Apply crossover and mutation to generate new paths
  Evaluate the fitness of the new paths
  Select the top Y paths to form the next generation
end for
Output: Optimal UGV path $\mathcal{P}_G^*$

Fig. 4 shows the UGV path optimized by GA, where the UGV efficiently covers high-risk zones while minimizing energy consumption. Future work will extend the optimization framework to incorporate the dynamic movement constraints of UAVs, including velocity and acceleration limits, to further enhance the realism and applicability of the model.

B. UAV Movement Optimization and Recharging Scheduling

UAV movement and recharging scheduling are essential for effective UAV-UGV cooperation in urban monitoring. UAVs perform multiple tasks, such as monitoring inaccessible areas, maintaining communication via RISs, and wirelessly recharging UGVs. These tasks require careful coordination to prevent UAVs from running out of energy while ensuring continuous UGV operation in high-risk zones. The UAV movement optimization problem is formulated as follows:

$$\begin{aligned}\max_{\{\mathcal{P}_V,\mathcal{P}_G\}} & \sum_{t=0}^{T}\sum_{i\in\mathcal{Z}}\sum_{(g,v)\in\mathcal{G}\times\mathcal{V}} z_i^{g,v}[t]\cdot\psi_i[t] \\ & + \left(\frac{1}{T}\sum_{t=0}^{T}\sum_{(g,v)\in\mathcal{G}\times\mathcal{V}} \aleph_g^v[t]\cdot R_g^{v,\mathrm{RIS}}[t]\right) \\ & + \frac{1}{T}\sum_{t=0}^{T}\frac{\sum_{g\in\mathcal{G}} E_g[t]^2+\sum_{v\in\mathcal{V}} E_v[t]}{G+V},\end{aligned} \tag{19}$$

Subjected to:

$$\begin{aligned}
&\text{C1:}\quad \|p_v[t]-p_v[t-1]\|^2 \le (V_v^{\max}\Delta)^2, \quad \forall v\in\mathcal{V},\forall t\in\mathcal{T},\\
&\text{C2:}\quad z_i^{g,v}[t]\in\{0,1,2\}, \quad \forall i\in\mathcal{Z},\forall t\in\mathcal{T},\forall g\in\mathcal{G},\forall v\in\mathcal{V},\\
&\text{C3:}\quad \sum_{i\in\mathcal{Z}} z_i^{g,v}[t]\cdot\psi_i[t]\ge\psi_{\min}, \quad \forall g\in\mathcal{G},\forall v\in\mathcal{V},\forall t\in\mathcal{T},\\
&\text{C4:}\quad E_v[t]\ge E_v^{\min}, \quad \forall v\in\mathcal{V},\forall t\in\mathcal{T},\\
&\text{C5:}\quad E_g[t]\ge E_g^{\min}, \quad \forall g\in\mathcal{G},\forall t\in\mathcal{T},\\
&\text{C6:}\quad d_v^{v'}[t]\ge d_{\min}, \quad \forall v'\ne v\in\mathcal{V},\forall t\in\mathcal{T},
\end{aligned}$$

The objective of (19) is to optimize UAV trajectories $\mathcal{P}_V = \{p_v[t], \forall v \in \mathcal{V}\}$ to maximize risk zone coverage, improve data relay, and minimize energy use. This optimization is challenging in unpredictable urban environments, requiring continuous operations and adaptation to varying energy demands and risk levels. **C1** ensures UAV velocity limits, **C2** defines zone occupancy, and **C3** prioritizes high-risk zones. **C4** and **C5** maintain energy levels above thresholds $E_v^{\min}$ and $E_g^{\min}$. **C6** prevents collisions by maintaining a minimum distance $d_{\min}$ between UAVs. Given the complexity of UAV movement and recharging, traditional methods struggle to provide real-time solutions. PPO, a DRL algorithm [40], is well-suited for high-dimensional, continuous control problems, enabling exploration and adapting to dynamic conditions and energy constraints.

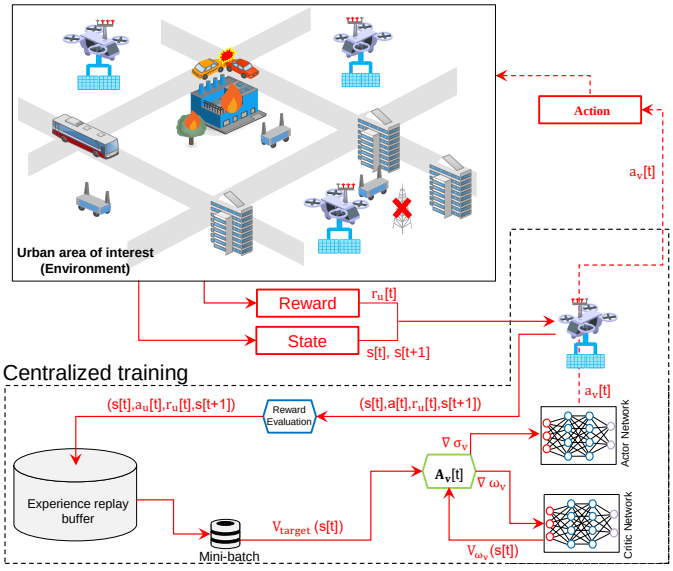

Fig. 5: ADVISE framework.

Our contribution, ADVISE, utilizes the PPO algorithm, a DRL method suited for continuous action space optimization. PPO operates within a Markov Decision Process (MDP) defined by the tuple $(\mathcal{S}, \mathcal{A}, \mathcal{R}, \mathcal{P})$, where $s[t] \in \mathcal{S}$ is the environment state at time t, $a[t] \in \mathcal{A}$ is the action taken, and $r[t] \in \mathcal{R}$ is the reward received. The transition probability $\mathcal{P}(s[t+1] \mid s[t], a[t])$ describes the likelihood of moving from state $s[t]$ to $s[t+1]$ after action $a[t]$. These components enable PPO to learn optimal policies by maximizing cumulative rewards. As shown in Fig. 5, each UAV v is controlled by an independent agent, optimizing movement and energy efficiency. The PPO-clip objective stabilizes learning by clipping the probability ratio between new and old policies. The PPO-clip objective for each UAV agent v is defined as:

$$\begin{aligned}L^{\mathrm{CLIP}}(\sigma_v) = \mathbb{E}_t\Bigg[\min\Bigg(&\frac{\pi_{\sigma_v}(a_v[t]|o_v[t])}{\pi_{\sigma_v^{\mathrm{old}}}(a_v[t]|o_v[t])}A_v[t],\\ &\mathrm{clip}\left(\frac{\pi_{\sigma_v}(a_v[t]|o_v[t])}{\pi_{\sigma_v^{\mathrm{old}}}(a_v[t]|o_v[t])},1-\epsilon,1+\epsilon\right)A_v[t]\Bigg)\Bigg],\end{aligned} \tag{20}$$

where $\pi_{\sigma_v}(a_v[t] \mid o_v[t])$ is the new policy's probability of taking action $a_v[t]$ given observation $o_v[t]$, and $\pi_{\sigma_v^{\mathrm{old}}}(a_v[t] \mid o_v[t])$ is the old policy's probability. $A_v[t]$ is the advantage function, indicating how much better the selected action $a_v[t]$

is compared to the expected one. ϵ controls the clipping range, while $\mathbb{E}_t$ denotes the expectation over time steps. This clipping mechanism ensures stable policy updates, preventing destabilizing changes, which makes PPO suitable for real-time UAV trajectory control. PPO works with a critic network evaluating the state-value function $V_{\omega_v}(s[t])$, which is used to calculate the advantage function, given by:

$$A_v[t] = \sum_{l=0}^{\infty} (\gamma\lambda)^l \left(r_v[t+l] + \gamma V_{\omega_v}(s[t+l+1]) - V_{\omega_v}(s[t+l])\right), \tag{21}$$

where γ is the discount factor that controls how much future rewards are weighted, and λ is the Generalized Advantage Estimation (GAE) factor, balancing bias and variance in the advantage estimation. Here, $r_v[t]$ represents the reward received by UAV v, and $V_{\omega_v}(s[t])$ is the state-value function estimated by the critic network. The temporal difference error $\delta_v[t] = r_v[t] + \gamma V_{\omega_v}(s[t+1]) - V_{\omega_v}(s[t])$ drives the updates to the critic network. The critic network is updated using the following loss function:

$$L_V(\omega_v) = \frac{1}{2}\mathbb{E}_t\left[\left(V_{\omega_v}(s[t]) - V_{\text{target}}(s[t])\right)^2\right], \tag{22}$$

where $V_{\text{target}}(s[t])$ is the target value for the state-value function. The actor and critic networks are updated using their respective gradients:

$$\nabla_{\sigma_v} = \frac{\partial L^{\text{CLIP}}(\sigma_v)}{\partial \sigma_v}, \quad \nabla_{\omega_v} = \frac{\partial L_V(\omega_v)}{\partial \omega_v}. \tag{23}$$

1) State Space: In the ADVISE framework, each UAV $v \in \mathcal{V}$ observes the environment through a unique state space at each time-slot t, formally defined as $s[t] = \{o_v[t], t \in \mathcal{T}, v \in \mathcal{V}\}$. The state space captures essential information required for UAV v to optimize its movement and energy management in real-time. The observation vector $o_v[t]$ at time-slot t includes the following components:

- $p_v[t]$: the position of UAV v.
- $E_v[t]$: the residual energy level of UAV v.
- $ST_v[t]$: a binary variable that indicates if UAV v is recharging its battery if $ST_v[t] = 1$, and $ST_v[t] = 0$ otherwise.
- $\sum_{i\in\mathcal{Z}}\sum_{g\in\mathcal{G}} z_i^{g,v}[t]$: zone occupancy, indicating whether UAV v, UGV g, or both are covering zone i.
- $\psi_i[t], \forall i \in \mathcal{Z}$: the risk scores of all zones in the area.
- $\sum_{g\in\mathcal{G}} \aleph_g^v[t] \cdot R_g^{v,\text{RIS}}[t]$: the data rate relayed by UAV v from UGVs.
- $p_g[t], \forall g \in \mathcal{G}$: positions of all UGVs.
- $E_g[t], \forall g \in \mathcal{G}$: residual energy levels of all UGVs.

Formally, the observation $o_v[t]$ for UAV v is defined as $o_v[t] = [p_v[t], E_v[t], \sum_{i\in\mathcal{Z}}\sum_{g\in\mathcal{G}} z_i^{g,v}[t], \psi_1[t], \ldots, \psi_Z[t], p_1[t], \ldots, p_G[t], E_1[t], \ldots, E_G[t], \sum_{g\in\mathcal{G}} \aleph_g^v[t] \cdot R_g^{v,\text{RIS}}[t], ST_v[t]]$. This information enables UAVs to make real-time decisions regarding movement, energy optimization, and zone coverage. To accelerate learning and improve data handling, each parameter is normalized between 0 and 1.

2) Action Space: The action space $\mathcal{A}$ for UAVs is divided into movement actions $\mathcal{A}_M[t]$, UAV recharging actions $\mathcal{A}_R[t]$, and UGV charging actions $\mathcal{A}_C[t]$. The action vector $a_v[t]$ for each UAV $v \in \mathcal{V}$ at time-slot t consists of:

- $\Upsilon_v[t] \in [0, 2\pi[$: horizontal orientation of UAV v.
- $d_v[t] \in [0, d_{max}]$: distance traveled by UAV v. If $d_v[t] = 0$, the UAV remains stationary.
- $h_v[t] \in [h_{\text{min}}, h_{\text{max}}]$: the altitude of UAV v.
- $\upsilon_v[t]$: a binary indicator where $\upsilon_v[t] = 1$ indicates active UGV charging, and $\upsilon_v[t] = 0$ otherwise.

During the UGV charging process, the action space $\mathcal{A}_C[t] = \{\Upsilon_v[t], d_v[t], h_v[t], \upsilon_v[t]\}$ is restricted such that $\Upsilon_v[t] = 0$, $d_v[t] = 0$, and the altitude remains constant. In this mode, the UAV hovers in place and maintains a constant altitude until charging is completed, with $\upsilon_v[t] = 1$. When UAV v needs to recharge itself at the central controller, located at coordinates $\{x_{\text{cc}}, y_{\text{cc}}, h_{\text{cc}}\}$, the action vector includes the azimuthal angle

$$\omega_v[t] = \arccos\left(\frac{x_v[t]x_{\text{cc}} + y_v[t]y_{\text{cc}}}{\sqrt{(x_v^2[t] + y_v^2[t])((x_{\text{cc}})^2 + (y_{\text{cc}})^2)}}\right),$$

the altitude $h_v[t] = h_{\text{cc}}$, and the distance $d_v[t] = \sqrt{(x_v[t] - x_{\text{cc}})^2 + (y_v[t] - y_{\text{cc}})^2}$ that the UAV travels to reach the central controller. At each time-slot t, the action vector $a_v[t] \in \hat{\mathcal{A}}[t]$ is defined by:

$$\hat{\mathcal{A}}[t] = \begin{cases} \mathcal{A}_M[t], & \text{If } \upsilon_v[t] = 0 \wedge ST_v[t] = 0, \\ \mathcal{A}_C[t], & \text{If } \upsilon_v[t] = 1 \wedge ST_v[t] = 0, \\ \mathcal{A}_R[t], & \text{If } \upsilon_v[t] = 0 \wedge E_v[t] < E_v^{max}, \end{cases} \tag{24}$$

where E_v^{max} is the maximum energy capacity of UAV v.

3) Reward: At each time-slot t, the reward $r_v[t]$ for UAV $v \in \mathcal{V}$ is calculated based on its performance in zone coverage, energy management, and communication with UGVs, incorporating penalties for inefficiencies. The reward function promotes efficient energy use, maximizes coverage of high-risk zones, and ensures reliable UAV-UGV communication.

$$r_v[t] = E_v[t] \cdot \left(\frac{\sum_{i\in\mathcal{Z}} z_i^{g,v}[t] \cdot \psi_i[t] + \sum_{g\in\mathcal{G}} \aleph_g^v[t] \cdot R_g^{v,\text{RIS}}[t]}{1 + \Sigma_v[t]}\right), \tag{25}$$

where $\Sigma_v[t]$ is the penalty incurred by UAV v for undesirable actions and is defined as:

$$\Sigma_v[t] = \rho_v^1[t] + \rho_v^2[t] + \rho_v^3[t], \tag{26}$$

where $\rho_v^1[t]$ penalizes UAV v for violating the minimum safety distance, $\rho_v^2[t]$ penalizes for leaving the operational area, and $\rho_v^3[t]$ penalizes for recharging when energy exceeds a threshold. These penalties are defined as:

$$\rho_v^1[t] = \begin{cases} \Lambda_1, & \text{if } d_v^{v'}[t] \le d_{\text{min}}, \forall v' \neq v \in \mathcal{V}, \\ 0, & \text{Otherwise}, \end{cases} \tag{27}$$

$$\rho_v^2[t] = \begin{cases} \Lambda_2, & \text{if } x_v(t) \wedge y_v(t) \notin [0, \mathbb{W}], \\ 0, & \text{Otherwise}. \end{cases} \tag{28}$$

$$\rho_v^3[t] = \begin{cases} \Lambda_3, & \text{if } E_v[t] > E_v^{\min} \wedge ST_v[t] = 1, \\ 0, & \text{Otherwise.} \end{cases} \tag{29}$$

In these formulas, Λ_1, Λ_2, and Λ_3 are penalty constants defined according to the severity of the action. The reward function penalizes inefficiencies, encouraging UAVs to focus on high-risk zones, optimize communication with UGVs, and minimize energy consumption and recharging.

4) ADVISE Algorithm: The ADVISE algorithm, based on the multi-agent PPO (MAPPO) framework, optimizes UAV movement and recharging scheduling in a multi-agent system. Each UAV operates as an independent agent, learning through real-time interaction with the environment (Line 1). Actor and critic networks are initialized with random parameters (Line 2). A centralized replay buffer stores transitions during UAV actions and rewards (Lines 5-9). At each time step, PPO stabilizes learning by clipping policy updates (Line 11) for smooth convergence. The algorithm iterates through PPO epochs, computing advantage function and policy/critic losses (Lines 12-19), followed by updating the networks using their gradients (Lines 17-18).

Algorithm 4: ADVISE Algorithm

1: Initialize actor networks $\pi_{\sigma_v}(o_v[t])$ and critic networks $V_{\omega_v}(s[t])$ for each UAV $v \in \mathcal{V}$ with random parameters σ_v and ω_v
2: Initialize centralized replay buffer $\mathcal{B}$ and set learning rate ν, discount factor γ, clipping parameter ϵ, and number of PPO epochs J
3: **for** each episode $ep = 1$ to I **do**
4: **for** each time step $t = 1$ to T **do**
5: **for** each UAV $v \in \mathcal{V}$ **do**
6: UAV v observes the state $o_v[t]$ and selects action $a_v[t] = \pi_{\sigma_v}(o_v[t])$
7: Execute action $a_v[t]$, observe reward $r_v[t]$, and obtain next state $o_v[t+1]$
8: Store transition $(o_v[t], a_v[t], r_v[t], o_v[t+1])$ in buffer $\mathcal{B}$
9: **end for**
10: **end for**
11: **for** each PPO epoch $j = 1$ to J **do**
12: **for** each UAV $v \in \mathcal{V}$ **do**
13: Sample a mini-batch of transitions from buffer $\mathcal{B}$
14: Compute advantage $A_v[t]$ using GAE (21)
15: Compute policy loss using (20)
16: Compute critic loss using (22)
17: Update actor parameters using: $\sigma_v \leftarrow \sigma_v - \nu \frac{\partial L^{\text{CLIP}}(\sigma_v)}{\partial \sigma_v}$
18: Update critic parameters using: $\omega_v \leftarrow \omega_v - \nu \frac{\partial L_V(\omega_v)}{\partial \omega_v}$
19: **end for**
20: **end for**
21: **end for**

V. Complexity Analysis

The computational complexity of the proposed algorithm is driven by the GA for UGV path optimization and the PPO algorithm for UAV trajectory planning. Both algorithms' time complexity is influenced by the number of iterations and the size of the state-action space, while their space complexity is determined by the storage of relevant optimization data. These complexities highlight the algorithm's scalability and efficient management of resources during optimization.

A. Complexity of GA

The GA for UGV path optimization involves key operations such as population initialization, fitness evaluation, selection, crossover, and mutation. With a population size P and $G_{\max}$ generations, each operation has a complexity of $\mathcal{O}(P)$ per generation. Therefore, the overall time complexity per iteration of the GA is:

$$\mathcal{O}(P \times G_{\max}), \tag{30}$$

The space complexity of the GA is proportional to the population size and the storage needed for each path, which depends on the number of zones and decision variables in the optimization. Thus, the space complexity is:

$$\mathcal{O}(P \times \text{size of each path}), \tag{31}$$

where the size of each path is proportional to the number of zones and variables (e.g., time steps, coordinates).

B. Complexity of PPO

The complexity of the PPO algorithm for UAV trajectory optimization is driven by iterative updates during training. The time and space complexity are both given by:

$$\mathcal{O}(I \times T \times |\mathcal{V}| \times (|\mathcal{S}| \times |\mathcal{A}|)), \tag{32}$$

where I is the number of episodes, T is the number of time steps, and $|\mathcal{V}|$ is the number of UAVs. This complexity reflects the required resources for storing trajectories, rewards, and policy parameters during the learning process.

The overall complexity of the system is influenced by the combined complexities of the GA for UGV path optimization and the PPO for UAV trajectory planning. The total time and space complexity can be represented as follows:

$$\mathcal{O}((P \times G_{\max}) + (I \times T \times |\mathcal{V}| \times (|\mathcal{S}| \times |\mathcal{A}|))). \tag{33}$$

The proposed system's dynamic adaptability introduces computational challenges due to continuous decision-making for path adjustments. PPO-based UAV trajectory optimization involves learning and policy updates, increasing complexity but improving adaptability. Similarly, GA-based UGV path optimization iterates over routes, balancing solution quality with execution time. To ensure real-time performance, adaptive update frequencies enable selective path updates based on triggers. By combining reinforcement learning and evolutionary optimization, the system manages the trade-off between adaptability and efficiency, ensuring scalability for large-scale urban deployments.

VI. Experiments and Results

We evaluate ADVISE by comparing its performance to DRL-based methods like Multi-Agent Deep Q-Network (MADQN) [41] and Deep Deterministic Policy Gradient (DDPG) [42], alongside baseline random and greedy strategies. The evaluation comprises two stages: (i) the learning phase, focused on convergence and training efficiency, and (ii) the testing phase, where real-time performance is assessed with the trained network parameters, evaluating real-time performance under identical environmental conditions for fairness. Implemented in Python 3.8.10 with TensorFlow 2.8.0, ADVISE is trained over 1000 episodes of 100 time steps each. Using the MAPPO framework, each UAV operates independently with actor and critic networks comprising four fully connected layers with ReLU activations and a tanh output layer for movement constraints. The centralized critic processes joint state-action pairs to enhance UAV coordination, optimizing high-risk zone monitoring and energy management. Table IV summarizes the simulation setup and key neural network parameters.

TABLE IV: Neural Network Parameters for ADVISE.

Neural Actor Network Parameters			
Layers	**Number**	**Size**	**Activation Function**
Input	1	$5+Z+2G$	-
Hidden	$\beth = 4$	400, 400, 300, 300	ReLU
Output	1	$\lvert\mathcal{A}_v\rvert = 4$	Tanh
Neural Critic Network Parameters			
Layers	**Number**	**Size**	**Activation Function**
Input	1	$V \times (5+Z+2G)$	-
Hidden	$\daleth = 4$	400, 400, 300, 300	ReLU
Output	1	1	-
Training Parameters			
Parameter		**Value**	
Replay buffer size $\mathcal{B}$		10^5	
Mini-batch size $\mathcal{M}$		256	
Optimizer		Adam	
Number of PPO epochs J		4	
GAE factor λ		0.95	
Number of time steps per episode T		100	
Total number of episodes		1000	
Penalty coefficients $\Lambda_1, \Lambda_2, \Lambda_3$		50	
Comparative methods		MADQN, DDPG, Random, Greedy	

Our simulations employed empirically tuned parameters for PPO, GA, and DE to ensure efficiency and stability. PPO used a learning rate (ν_{σ_v}) of 0.0002 for the actor, 0.0001 for the critic (ν_{ω_v}), a discount factor ($\gamma = 0.99$), and a clipping parameter ($\epsilon = 0.2$) for UAV trajectory planning. GA parameters included a mutation rate of 0.02 and a crossover probability of 0.85 to balance exploration and exploitation in UGV path planning. DE was configured with a mutation factor ($F = 0.8$) and crossover rate ($CR = 0.9$) to optimize RIS phase shifts while preventing local minima. Extensive trials validated these settings, ensuring optimal trade-offs in convergence speed, solution quality, and adaptability across energy, communication, and coverage performance. Simulations are conducted in a smart city with a 15 km width, covering 225 km^2. Twenty UAVs monitor high-risk zones, while 50 UGVs patrol autonomously. UAVs operate between 100 and 150 meters, providing reliable communication and energy transfer to UGVs via RIS-enabled systems. Table V lists the main simulation parameters.

TABLE V: Simulation Parameters.

Environment Parameters			
Parameter	**Description**	**Value**	**Units**
Area	Urban monitoring area of width $\mathbb{W}$	15×15	km^2
h_{UAV}	Altitude of UAVs	100 – 150	m
P_g	Transmit power of UGV$_g$	-10 – 20	dBm
$V_u^{\max}$	Maximum velocity of UAV$_u$	12	m/s
$V_g^{\max}$	Maximum velocity of UGV$_g$	2	m/s
η	Path loss exponent	2.5	Dimensionless
ξ	Energy conversion efficiency	0.3	Dimensionless
$M \times N$	RIS reflecting elements	64×64	Elements
ϱ_i	Phase shift of the i-th element	$[0, 2\pi)$	Radians
P_{RIS}	Power consumption per RIS element	0.05	W
σ^2	Noise power	-95	dBm
UGV Parameters			
Parameter	**Description**	**Value**	**Units**
Battery Capacity	Battery capacity of UGV$_g$	2000 – 5000	mAh
Sensor Range	Detection range of UGVs	50	m
Edge Computing Parameters			
$D_g[t]$	Computing task size of UGV$_g$	10 – 200	MB
C_g	CPU cycles number of UGV$_g$	1000 – 5000	Cycles/bit
$f_g[t]$	Computation frequency of UGV$_g$	2.5	GHz
κ_g	Processor efficiency of UGV$_g$	10^{-12}	Joules/Hz$^{\beta-1}$
β	Power consumption exponent	2.0	Dimensionless

A. Learning phase analysis

During learning, the system explores using random actions, optimizing performance over time. The ADVISE framework's reward, shown in Fig. 6, steadily increases and stabilizes around 300 episodes, indicating effective UAV-UGV coordination. Initially, random exploration diversifies the experience pool, transitioning to exploitation as long-term rewards are prioritized. The observed stability after convergence reflects the agents' ability to balance energy, positioning, and communication, ensuring reliable, scalable performance in urban monitoring.

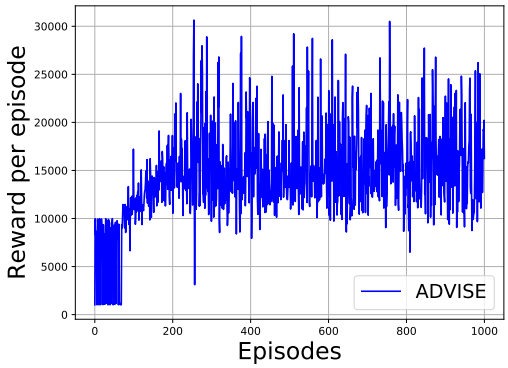

Fig. 6: Reward per episode of ADVISE framework.

Fig. 7 highlights ADVISE's superior performance over MADQN and DDPG in accumulated rewards, data rates, and energy efficiency. In Fig. 7(a), ADVISE achieves higher accumulated rewards due to its balanced exploration-exploitation strategy, while MADQN and DDPG are limited by design constraints. MADQN's discrete actions restrict decision-making, and DDPG suffers from learning instability without policy regularization. In Fig. 7(b), ADVISE excels in data rates by dynamically adjusting UAV paths, unlike MADQN and DDPG, which struggle with real-time adaptability. Fig. 7(c) shows ADVISE maintaining superior UAV residual energy through optimized recharging and path planning, whereas MADQN and DDPG quickly drain

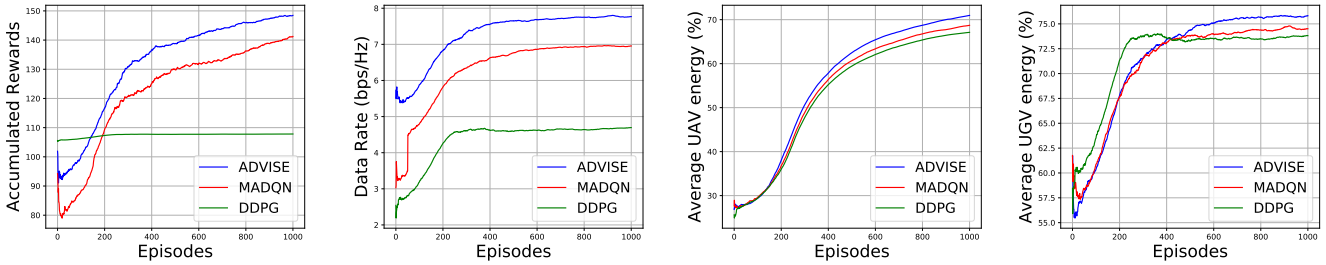

(a) Accumulated rewards. (b) Data rates. (c) UAV residual energy (%). (d) UGV residual energy (%).

Fig. 7: Convergence results of ADVISE in terms of rewards, data rates, and UAV and UGV residual energy.

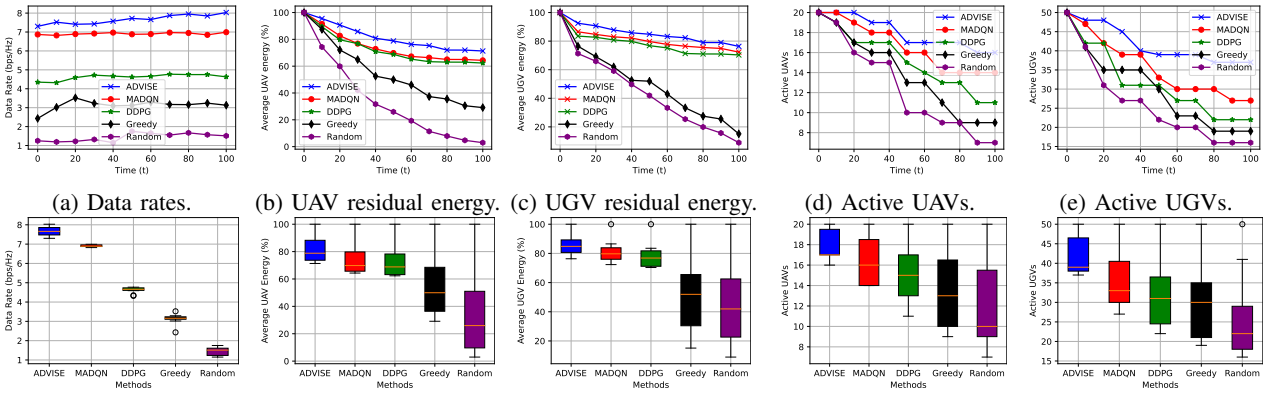

(a) Data rates. (b) UAV residual energy. (c) UGV residual energy. (d) Active UAVs. (e) Active UGVs.

(f) Data rates. (g) UAV residual energy. (h) UGV residual energy. (i) Active UAVs. (j) Active UAVs.

Fig. 8: Performance of ADVISE in terms of data rates and UAV and UGV residual energy.

energy. Finally, Fig. 7(d) demonstrates ADVISE's efficient energy management for UGVs, ensuring longer coverage compared to MADQN and DDPG, which lack adaptive energy strategies. These limitations emphasize ADVISE's adaptability and scalability for 6G urban monitoring.

B. Testing phase analysis

During the testing phase, ADVISE effectively applies the refined policies from training, consistently outperforming MADQN, DDPG, and baseline strategies across all key metrics, as shown in Fig. 8. ADVISE achieves superior data rates (*c.f.,* Figs. 8(a), 8(f)), skillfully managing communication and UV relaying to the central controller, while the competitors lag behind, limited by static decision frameworks that lack adaptive capacity. In terms of energy management, ADVISE demonstrates markedly higher residual energy for both UAVs (*c.f.,* Figs. 8(b), 8(g)) and UGVs (*c.f.,* Figs. 8(c), 8(h)), supporting longer operational spans. MADQN and DDPG, by contrast, rapidly deplete energy reserves due to less sophisticated, rigid energy policies. Additionally, ADVISE maintains a greater density of active UAVs and UGVs (*c.f.,* Figs. 8(d), 8(i), 8(e), 8(j)) throughout mission durations, while MADQN and DDPG face difficulties in coordination and energy efficiency, leading to a quicker reduction in active agents. These outcomes underscore ADVISE's robust balancing of data throughput, energy optimization, and adaptive coordination, which together secure its efficacy in dynamic urban monitoring tasks.

The results in Fig. 9 highlight the superior performance of the GA-based system, particularly when integrated with UAVs, compared to greedy and random strategies. As shown in Fig. 9(a), the GA-based system with UAVs achieves the highest coverage of high-risk zones, benefiting from aerial support for improved coordination and monitoring. Even without UAVs, it outperforms greedy and random approaches but with reduced adaptability and coverage. In terms of energy efficiency, Fig. 9(b) illustrates that the GA-based system with UAVs sustains higher UGV residual energy over time due to optimized task allocation and energy management. Without UAVs, energy depletion is faster but still superior to greedy and random methods, which exhibit rapid exhaustion due to inefficient decision-making. Lastly, Fig. 9(c) shows that the GA-based system with UAVs minimizes UGV travel distances, enhancing energy efficiency and task execution. Without UAVs, UGVs travel further but remain more efficient than competing strategies, whereas greedy and random methods result in excessive travel distances, underscoring their inefficiency in urban monitoring.

Fig. 10 compares ADVISE with Ref. [20], focusing on cooperative UAV-UGV systems in multi-agent path planning. As shown in Fig. 10(a), ADVISE achieves superior high-risk zone coverage through real-time UAV trajectory optimization via PPO and dynamic RIS-assisted coordination, whereas Ref. [20] lacks adaptive coordination and reliable communication, leading to suboptimal coverage. Additionally, Fig. 10(b) illustrates that ADVISE sustains higher UGV residual

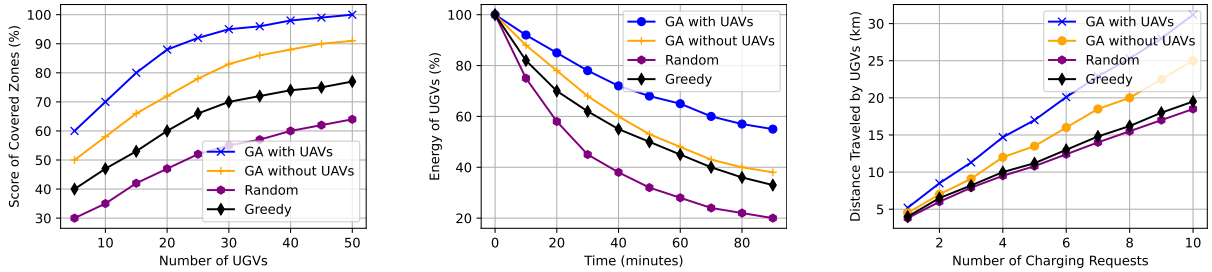

(a) Score of covered zones (%). (b) UGV residual energy (%). (c) Distance traveled by UGVs (km).

Fig. 9: Performance of ADVISE in terms of Score, Energy, and Distance traveled.

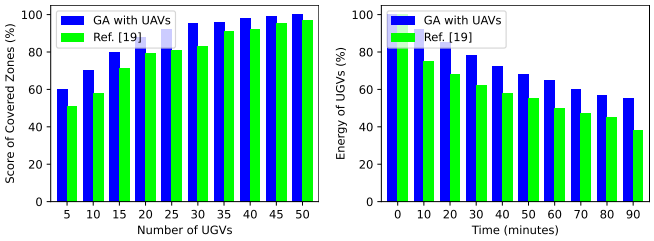

(a) Score of covered zones (%). (b) UGV residual energy (%).

Fig. 10: Performance of ADVISE vs. Ref. [20].

energy by dynamically recharging UGVs and optimizing path planning, while Ref. [20] lacks such mechanisms, resulting in faster energy depletion. These results highlight ADVISE's superior performance in both coverage and energy efficiency, ensuring greater adaptability and extended operational capabilities.

VII. Conclusion and Discussions

This paper introduces ADVISE, a UAV-UGV cooperative framework integrating RIS-equipped UAVs and UGVs for real-time urban monitoring in 6G networks. ADVISE tackles energy management, communication reliability, and dynamic task allocation through multi-agent PPO for UAV trajectory optimization and a GA-based approach for UGV path planning. Compared to MADQN, DDPG, greedy, and random strategies, ADVISE outperforms in coverage, data rates, and energy efficiency, with UAV integration enhancing monitoring and communication in high-risk areas. Simulations confirm ADVISE's capability to maintain a higher density of active UAVs and UGVs, ensuring continuous monitoring and efficient task execution. While ADVISE offers a scalable solution for urban monitoring, real-world deployment challenges remain. Future work will focus on enhancing energy efficiency through kinetic energy recovery (e.g., regenerative braking for UGVs, airborne energy harvesting for UAVs), AI-driven dynamic energy management, and multi-modal learning for improved UAV-UGV coordination. LiDAR-based obstacle detection and federated learning will further optimize navigation and decision-making, while game-theoretic models will refine strategic coordination. Additionally, resilient communication protocols will be developed to ensure robust connectivity in dense urban environments.

In future work, we will conduct a comprehensive sensitivity analysis to examine the impact of key hyperparameters, such as PPO learning rates, GA mutation rates, and DE crossover probabilities, on system efficiency and adaptability, helping refine optimization strategies for a balanced trade-off between performance, energy efficiency, and computational cost. To address scalability, we will implement tiny reinforcement learning (TinyRL) for UAVs, enabling lightweight neural networks to process an increasing number of agents efficiently while minimizing computational complexity and energy consumption. Furthermore, adaptive task offloading mechanisms will be explored to dynamically distribute computational workloads among UAVs, UGVs, and edge servers, optimizing resource utilization under varying conditions. From an infrastructure perspective, we will focus on ensuring seamless integration with urban systems, enhancing network connectivity and deployment feasibility, while also prioritizing regulatory compliance to align with airspace safety standards for large-scale UAV-UGV deployment. To improve UAV-UGV coordination, we will integrate multi-objective optimization algorithms to balance trade-offs between coverage, communication reliability, and energy efficiency, leveraging metaheuristic and evolutionary algorithms for real-time adjustments. Dynamic weight adjustments will enable PPO to optimize UAV flight paths based on real-time feedback, while GA will adapt UGV patrol routes under fluctuating conditions, ensuring operational efficiency. Stable communication will be maintained through RIS-equipped UAVs dynamically adjusting beamforming strategies, and UAVs will autonomously schedule UGV recharging to support continuous mission execution. Real-time optimization remains crucial to ADVISE's adaptability, with PPO for UAV trajectory planning, GA for UGV path optimization, and DE for RIS phase shift adjustments ensuring seamless adaptation to dynamic environments. Future research will further enhance these capabilities by implementing multi-agent TinyRL for decentralized UAV-UGV learning, improving system-wide coordination and decision-making, while digital twin environments will be developed to simulate large-scale real-world conditions, refining optimization techniques before deployment. Finally, real-world testing and hardware-in-the-loop validation will rigorously assess ADVISE's effectiveness in complex urban environments, integrating multi-modal learning techniques such as optical, infrared, LiDAR, and wireless data fusion to

enhance UAV-UGV perception and adaptability. Additionally, federated learning and decentralized decision-making will be explored to optimize performance while reducing reliance on centralized computation, improving scalability and resilience for long-term urban monitoring. Large-scale field experiments and hardware-in-the-loop simulations will be conducted to validate ADVISE's real-world efficiency and adaptability, ensuring its viability for next-generation 6G-enabled intelligent urban infrastructure.

ACKNOWLEDGEMENT

The Researchers would like to thank the Deanship of Graduate Studies and Scientific Research at Qassim University for financial support (QU-APC-2024-9/1).

REFERENCES

[1] Y. Liu, L. Huo, J. Wu, and A. K. Bashir, "Swarm learning-based dynamic optimal management for traffic congestion in 6G-driven intelligent transportation system," *IEEE Transactions on Intelligent Transportation Systems*, vol. 24, no. 7, pp. 7831–7846, 2023.

[2] S. Hu, X. Yuan, W. Ni, X. Wang, and A. Jamalipour, "Visual camouflage and online trajectory planning for unmanned aerial vehicle-based disguised video surveillance: Recent advances and a case study," *IEEE Vehicular Technology Magazine*, vol. 18, no. 3, pp. 48–57, 2023.

[3] P. Yi, L. Zhu, Z. Xiao, R. Zhang, Z. Han, and X.-G. Xia, "Trajectory Design and Resource Allocation for Multi-UAV Communications Under Blockage-Aware Channel Model," *IEEE Transactions on Communications*, vol. 72, no. 4, pp. 2324–2338, 2023.

[4] J. C. N. Bittencourt, D. G. Costa, P. Portugal, and F. Vasques, "A Survey on Adaptive Smart Urban Systems," *IEEE Access*, vol. 12, pp. 102 826–102 850, 2024.

[5] Q. Chang, D. Tao, J. Wang, and R. Gao, "Deep Compressed Sensing based Data Imputation for Urban Environmental Monitoring," *ACM Transactions on Sensor Networks*, vol. 20, no. 1, pp. 1–21, 2023.

[6] N. R. Zema, E. Natalizio, L. D. P. Pugliese, and F. Guerriero, "3D trajectory optimization for multimission UAVs in smart city scenarios," *IEEE Transactions on Mobile Computing*, vol. 23, no. 1, pp. 1–11, 2022.

[7] M. A. Javed, T. N. Nguyen, J. Mirza, J. Ahmed, and B. Ali, "Reliable communications for cybertwin-driven 6G IoVs using intelligent reflecting surfaces," *IEEE Transactions on Industrial Informatics*, vol. 18, no. 11, pp. 7454–7462, 2022.

[8] I. Donevski, M. Virgili, N. Babu, J. J. Nielsen, A. J. Forsyth, C. B. Papadias, and P. Popovski, "Sustainable Wireless Services with UAV Swarms Tailored to Renewable Energy Sources," *IEEE Transactions on Smart Grid*, vol. 14, no. 4, pp. 3296–3308, 2022.

[9] P. Chen, L. Luo, D. Guo, X. Luo, X. Li, and Y. Sun, "Secure Task Offloading for Rural Area Surveillance Based on UAV-UGV Collaborations," *IEEE Transactions on Vehicular Technology*, vol. 73, no. 1, pp. 923–937, 2023.

[10] H. Cao, W. Zhu, Z. Chen, Z. Sun, and D. O. Wu, "Energy-delay tradeoff for dynamic trajectory planning in priority-oriented UAV-aided IoT networks," *IEEE Transactions on Green Communications and Networking*, vol. 7, no. 1, pp. 158–170, 2022.

[11] J. Zhao, Y. Nie, H. Zhang, and F. R. Yu, "A UAV-aided vehicular integrated platooning network for heterogeneous resource management," *IEEE Transactions on Green Communications and Networking*, vol. 7, no. 1, pp. 512–521, 2023.

[12] S. Brotee, F. Kabir, M. A. Razzaque, P. Roy, M. Mamun-Or-Rashid, M. R. Hassan, and M. M. Hassan, "Optimizing uav-ugv coalition operations: A hybrid clustering and multi-agent reinforcement learning approach for path planning in obstructed environment," *Ad Hoc Networks*, vol. 160, p. 103519, 2024.

[13] Q. Chen, Z. Guo, W. Meng, S. Han, C. Li, and T. Q. Quek, "A survey on resource management in joint communication and computing-embedded SAGIN," *IEEE Communications Surveys & Tutorials*, 2024.

[14] J. Li, Y. Cheng, J. Zhou, J. Chen, Z. Liu, S. Hu, and V. C. Leung, "Energy-efficient ground traversability mapping based on UAV-UGV collaborative system," *IEEE Transactions on Green Communications and Networking*, vol. 6, no. 1, pp. 69–78, 2021.

[15] G. Niu, L. Wu, Y. Gao, and M.-O. Pun, "Unmanned aerial vehicle (UAV)-assisted path planning for unmanned ground vehicles (UGVs) via disciplined convex-concave programming," *IEEE Transactions on Vehicular Technology*, vol. 71, no. 7, pp. 6996–7007, 2022.

[16] X. Cai, B. Schlotfeldt, K. Khosoussi, N. Atanasov, G. J. Pappas, and J. P. How, "Energy-aware, collision-free information gathering for heterogeneous robot teams," *IEEE Transactions on Robotics*, vol. 39, no. 4, pp. 2585–2602, 2023.

[17] H. Peng and L.-C. Wang, "Energy harvesting reconfigurable intelligent surface for UAV based on robust deep reinforcement learning," *IEEE Transactions on Wireless Communications*, vol. 22, no. 10, pp. 6826–6838, 2023.

[18] X. Qin, Z. Song, T. Hou, W. Yu, J. Wang, and X. Sun, "Joint optimization of resource allocation, phase shift, and UAV trajectory for energy-efficient RIS-assisted UAV-enabled MEC systems," *IEEE Transactions on Green Communications and Networking*, vol. 7, no. 4, pp. 1778–1792, 2023.

[19] P. Wang, W. Mei, J. Fang, and R. Zhang, "Target-mounted intelligent reflecting surface for joint location and orientation estimation," *IEEE Journal on Selected Areas in Communications*, vol. 41, no. 12, pp. 3768–3782, 2023.

[20] J. Zhang, Y. Wu, and M. Zhou, "Cooperative Dual-Task Path Planning for Persistent Surveillance and Emergency Handling by Multiple Unmanned Ground Vehicles," *IEEE Transactions on Intelligent Transportation Systems*, 2024.

[21] Z. Li, Y. Guo, G. Wang, J. Sun, and K. You, "Informative Trajectory Planning for Air-Ground Cooperative Monitoring of Spatiotemporal Fields," *IEEE Transactions on Automation Science and Engineering*, 2024.

[22] M. Xi, H. Dai, J. He, W. Li, J. Wen, S. Xiao, and J. Yang, "A lightweight reinforcement learning-based real-time path planning method for unmanned aerial vehicles," *IEEE Internet of Things Journal*, vol. 11, no. 12, pp. 21 061–21 071, 2024.

[23] B. Fan, L. Jiang, Y. Chen, Y. Zhang, and Y. Wu, "UAV assisted traffic offloading in air ground integrated networks with mixed user traffic," *IEEE Transactions on Intelligent Transportation Systems*, vol. 23, no. 8, pp. 12 601–12 611, 2021.

[24] T. C. Lam, N.-S. Vo, M.-P. Bui, C. D. T. Thai, H. Jung, and V.-C. Phan, "Service Time-aware Caching, Power Allocation, and 3D Trajectory Optimised Multimedia Content Delivery in UAV-assisted IoT Networks," *IEEE Transactions on Vehicular Technology*, 2024.

[25] J. Du, T. Lin, C. Jiang, Q. Yang, C. F. Bader, and Z. Han, "Distributed Foundation Models for Multi-Modal Learning in 6G Wireless Networks," *IEEE Wireless Communications*, vol. 31, no. 3, pp. 20–30, 2024.

[26] A. Li, S. Ni, Y. Chen, J. Chen, X. Wei, L. Zhou, and M. Guizani, "Cross-modal object detection via UAV," *IEEE Transactions on Vehicular Technology*, vol. 72, no. 8, pp. 10 894–10 905, 2023.

[27] P. Ren, J. Wang, Z. Tong, J. Chen, P. Pan, and C. Jiang, "Federated Learning via Non-Orthogonal Multiple Access for UAV-Assisted Internet of Things," *IEEE Internet of Things Journal*, vol. 11, no. 17, pp. 27 994–28 006, 2024.

[28] X. Li, M. Zhang, H. Chen, C. Han, L. Li, D.-T. Do, S. Mumtaz, and A. Nallanathan, "UAV-enabled multi-pair massive MIMO-NOMA relay systems with low-resolution ADCs/DACs," *IEEE Transactions on Vehicular Technology*, vol. 73, no. 2, pp. 2171–2186, 2023.

[29] S. Lin, Y. Zou, and D. W. K. Ng, "Ergodic Throughput Maximization for RIS-Equipped-UAV-Enabled Wireless Powered Communications With Outdated CSI," *IEEE Transactions on Communications*, vol. 72, no. 6, pp. 3634–3650, 2024.

[30] Y. Yu, X. Liu, Z. Liu, and T. S. Durrani, "Joint trajectory and resource optimization for RIS assisted UAV cognitive radio," *IEEE Transactions on Vehicular Technology*, vol. 72, no. 10, pp. 13 643–13 648, 2023.

[31] Y. Cai, Z. Wei, S. Hu, C. Liu, D. W. K. Ng, and J. Yuan, "Resource allocation and 3D trajectory design for power-efficient IRS-assisted UAV-NOMA communications," *IEEE Transactions on Wireless Communications*, vol. 21, no. 12, pp. 10 315–10 334, 2022.

[32] C. Wu, F. Ke, X. Yang, M. Wen, D. Li, and X. Zhang, "Joint energy and information precoding for NOMA-based WPCNs aided by reconfigurable intelligent surface," *IEEE Transactions on Vehicular Technology*, vol. 72, no. 11, pp. 14 559–14 572, 2023.

[33] P.-Q. Huang, Y. Zhou, K. Wang, and B.-C. Wang, "Placement optimization for multi-IRS-aided wireless communications: An adaptive differential evolution algorithm," *IEEE Wireless Communications Letters*, vol. 11, no. 5, pp. 942–946, 2022.

[34] V. Khodamoradi, A. Sali, O. Messadi, A. Khalili, and B. B. M. Ali, "Energy-efficient massive MIMO SWIPT-enabled systems," *IEEE*

Transactions on Vehicular Technology, vol. 71, no. 5, pp. 5111–5127, 2022.

[35] U. C. Cabuk, M. Tosun, O. Dagdeviren, and Y. Ozturk, "Modeling Energy Consumption of Small Drones for Swarm Missions," *IEEE Transactions on Intelligent Transportation Systems*, vol. 25, no. 8, pp. 10 176–10 189, 2024.

[36] Y. Zhang, J. Lyu, and L. Fu, "Energy-efficient trajectory design for UAV-aided maritime data collection in wind," *IEEE Transactions on Wireless Communications*, vol. 21, no. 12, pp. 10 871–10 886, 2022.

[37] F. S. Abkenar, P. Ramezani, S. Iranmanesh, S. Murali, D. Chulerttiyawong, X. Wan, A. Jamalipour, and R. Raad, "A survey on mobility of edge computing networks in IoT: State-of-the-art, architectures, and challenges," *IEEE Communications Surveys & Tutorials*, vol. 24, no. 4, pp. 2329–2365, 2022.

[38] G. Huang, X. Yuan, K. Shi, Z. Liu, and X. Wu, "A 3-D multi-object path planning method for electric vehicle considering the energy consumption and distance," *IEEE Transactions on Intelligent Transportation Systems*, vol. 23, no. 7, pp. 7508–7520, 2021.

[39] N. Wang, X. Liang, Z. Li, Y. Hou, and A. Yang, "PSE-D model-based cooperative path planning for UAV&USV systems in anti-submarine search missions," *IEEE Transactions on Aerospace and Electronic Systems*, 2024.

[40] J. Schulman, F. Wolski, P. Dhariwal, A. Radford, and O. Klimov, "Proximal policy optimization algorithms," *arXiv preprint arXiv:1707.06347*, 2017.

[41] Y. Liu, J. Yan, and X. Zhao, "Deep-reinforcement-learning-based optimal transmission policies for opportunistic UAV-aided wireless sensor network," *IEEE Internet of Things Journal*, vol. 9, no. 15, pp. 13 823–13 836, 2022.

[42] T. Lillicrap, "Continuous control with deep reinforcement learning," *arXiv preprint arXiv:1509.02971*, 2015.

Omar Sami Oubbati is an Associate Professor at the University Gustave Eiffel in the region of Paris, France. He is a member of the Gaspard Monge Computer Science laboratory (LIGM CNRS UMR 8049). He received his degree of Engineer (2010), M.Sc. in Computer Engineering (2011), M.Sc. degree (2014), and a PhD in Computer Science (2018), all from University of Laghouat, Algeria. From Oct. 2016 to Oct. 2017, he was a Visiting PhD Student with the Laboratory of Computer Science, University of Avignon, France. He spent 6 years as an Assistant Professor at the Electronics department, University of Laghouat, Algeria and a Research Assistant in the Computer Science and Mathematics Lab (LIM) at the same university. His main research interests are in Flying and Vehicular ad hoc networks, Energy harvesting and Mobile Edge Computing, Energy efficiency and Internet of Things (IoT). He is the recipient of the 2019 Best Survey Paper for Vehicular Communications (Elsevier). He has actively served as a reviewer for flagship IEEE Transactions journals and conferences, and participated as a Technical Program Committee Member for a variety of international conferences, such as IEEE ICC, IEEE CCNC, IEEE ICCCN, IEEE WCNC, IEEE ICAEE, and IEEE ICAIT. He serves on the editorial board of Vehicular Communications Journal of Elsevier and Communications Networks Journal of Frontiersin. He has also served as guest editor for a number of international journals. He is a member of the IEEE and IEEE Communications Society.

Jamal Alotaibi received the B.S. degree in Computer engineering from Qassim University, in 2012. He joined Wayne state university 2016 and received M. S. degree in Electrical and Computer Engineering. He worked in STC the telecommunication company as networks engineering. Dr. Alotaibi worked as Software engineering at Ford Company MI, from 2018 till 2022. In 2022, he received his Ph.D. degree from Electrical and Computer Engineering Department, College of Engineering, Wayne State University. Dr. Alotaibi research interests include Internet of Things (IoT) applications and security, computer networks, wireless and mobile networks, machine learning, and cybersecurity. Dr. Alotaibi currently working as Assistant Professor in department of computer engineering at Qassim university.

Fares Alromithy is an Assistant Professor of Electrical and Computer Engineering at the University of Tabuk, Saudi Arabia. He earned his B.S. in Electrical Engineering from Indiana University – Purdue University Indianapolis in 2009, followed by an M.S. from Wayne State University, and a Ph.D. from Oakland University. Dr. Alromithy's research explores advanced smart sensors, microelectromechanical systems (MEMS), nanoelectronics, and integrated microsystems. His work focuses on developing miniature, innovative sensors with applications in sectors like healthcare, telecommunications, and environmental monitoring.

Mohammed Atiquzzaman received the M.S. and Ph.D. degrees in electrical engineering and electronics from the University of Manchester, U.K., in 1984 and 1987, respectively. He currently holds the Edith J. Kinney Gaylord Presidential Professorship with the School of Computer Science, University of Oklahoma, USA. His research has been funded by the National Science Foundation, National Aeronautics and Space Administration, U.S. Air Force, Cisco, and Honeywell. He coauthored Performance of TCP/IP Over ATM Networks and has authored more than 300 refereed publications. His current research interests include areas of transport protocols, wireless and mobile networks, ad hoc networks, satellite networks, power-aware networking, and optical communications. He Co-Chaired the IEEE High Performance Switching and Routing Symposium (2003, 2011), IEEE GLOBECOM and ICC (2014, 2012, 2010, 2009, 2007, and 2006), IEEE VTC (2013), and SPIE Quality of Service Over Next Generation Data Networks conferences (2001, 2002, and 2003). He was the Panels Co-Chair of INFOCOM'05, and has been on the program committee of many conferences, such as INFOCOM, GLOBECOM, ICCCN, ICCIT, Local Computer Networks, and serves on the review panels at the National Science Foundation. He was the Chair of the IEEE Communication Society Technical Committee on Communications Switching and Routing. He received the IEEE Communication Society's Fred W. Ellersick Prize and the NASA Group Achievement Award for outstanding work to further NASA Glenn Research Center's efforts in the area of the Advanced Communications/Air Traffic Management's Fiber Optic Signal Distribution for Aeronautical Communications project. He received from IEEE the 2018 Satellite and Space Communications Technical Recognition Award for valuable contributions to the Satellite and Space Communications scientific community. He also received the 2017 Distinguished Technical Achievement Award from IEEE Communications Society in recognition of outstanding technical contributions and services in the area of communications switching and routing. He is the Editor in Chief of Journal of Networks and Computer Applications, the founding Editor in Chief of Vehicular Communications, and serves served on the editorial boards of many journals, including IEEE Communications Magazine, IEEE Journal on Selected Areas in Communications, IEEE Transactions on Mobile Computing, Real Time Imaging Journal, Journal of Sensor Networks, and International Journal of Communication Systems.

Mohammad Rashed Altimania is an Assistant Professor at University of Tabuk, Saudi Arabia. In March 2010, He completed his Bachelor of Science Degree in Electrical Engineering from Qassim University. He obtained a Master of Science degree in Electrical Engineering from the University of Tennessee at Chattanooga in May 2014. He received his Ph.D. Degree in Electrical Engineering from Missouri University of Science and Technology (Rolla, MO, USA) in 2020. His current research interests include Modeling and Design of Power Electronic Converters, Switched-Capacitor Converters, Power and Energy systems, Renewable Energy Harvesting (Wind and Solar Energy), Smart Grids, Virtual Power Plants, Distributed Generations, and Solar Desalination.